Dependency of the slip phenomenon on the inertial forces inside radial runners

Cite as: AIP Conference Proceedings **2191**, 020034 (2019); https://doi.org/10.1063/1.5138767
Published Online: 17 December 2019

Tommaso Capurso, Michele Stefanizzi, Giuseppe Pascazio, Sergio Mario Camporeale, and Marco Torresi

Dependency of the Slip Phenomenon on the Inertial Forces Inside Radial Runners

Tommaso Capurso[1,a)], Michele Stefanizzi[1], Giuseppe Pascazio[1], Sergio Mario Camporeale[1] and Marco Torresi[1]

[1]*Department of Mechanics, Mathematics and Management, Polytechnic University of Bari, Via E. Orabona, 4, 70125, Bari, Italy*

[a)]Corresponding author: tommaso.capurso@poliba.it

Abstract. The slip phenomenon consists in the deviation of the fluid flow (relative velocity vector) with respect to the blade congruent angles and is mainly due to the finite number of blades. For this reason, slip becomes significant in pumps operating as turbines (PaTs) being characterized by a lower number of blades compared to conventional turbines highlighting a shortcoming of these devices in energy recovery applications. Even though this topic has been widely investigated in the past for centrifugal pumps, it has been often neglected for hydraulic turbine applications. As described in the literature, a counter rotating vortex (known as eddy vortex) develops inside each vane of a rotating machine and its effect can be superimposed to the main flow characteristics. Moreover, the relative vorticity magnitude, which is twice the angular velocity under the hypothesis of inviscid, incompressible and irrotational flow, is constant regardless of the number of vanes. In this work, 3D inviscid steady flow numerical simulations of a purely radial impeller with zero-thickness blades, being designed according to a logarithmic spiral law, have been carried out with the purpose of bringing out the relationship between the flow deviation and the number of blades, neglecting viscous effects which could hinder the inertial ones. The results show a local deviation of the streamline downstream of the trailing edge when the flow is not confined by the blades. The effect of the flow deviation has been also evaluated by calculating the hydraulic performance of the runners. Four different runners have been investigated (with 28, 14, 7 and 3 blades) at their design point and rotating at two different angular velocities. This allowed to correlate the deviation with the inertial effect and to propose a least-squares fitting curve. As shown in previous works, the inclusion of the slip correction factor in 1-D PaT performance prediction models enhances their accuracy.

INTRODUCTION

The slip phenomenon has been widely discussed and investigated in the past inside radial and mixed flow turbomachinery [1, 2, 3, 4]. This affects the performance of centrifugal pumps, compressors and to a less extent turbines since they are characterized by a higher number of blades. The main reason behind this phenomenon is the finite number of blades which determines a deviation with respect to the blade congruent angles of the flow towards the vane exit. This leads to a reduction of the ideal work exchanged with the fluid. Nevertheless, due to the velocity and pressure distribution around the blades, on their pressure and suction sides, the work transfer is only made possible through a deviation between the blade and flow angles at the outlet of the vane [5, 6].

Due to the increasingly world energy demand and the need to improve the energy efficiency of complex systems, in the last decades pumps operating as turbines (PaTs) have been widely employed in various engineering fields. For instance, they are applied into water distribution networks (WDN) and industrial process plants [7, 8] in substitution of pressure relieve valves (PRV), which are used for regulation but necessarily determine a waste of energy [9, 10, 11].

Being actually pumps, PaTs are characterized by a low number of blades (typically from 5 to 8 blades) so they are particularly subject to slip. In order to give a deep insight in the inertial causes of the slip phenomenon, this work deals with the inviscid flow through a zero-thickness blade purely radial impeller (quasi 2-D configuration). Thus the flow is characterized only by radial and tangential directions while the axial direction is negligible making the investigation easier with respect to the more complex mixed axial-radial flow impeller case [12].

Recently, Xiaohui et al. [13] have shown the effect of the slip phenomenon but at the inlet of the impeller under

74th ATI National Congress
AIP Conf. Proc. 2191, 020034-1–020034-10; https://doi.org/10.1063/1.5138767
Published by AIP Publishing. 978-0-7354-1938-4/$30.00

off-design conditions. Herein, the slip phenomenon is investigated at the vane outlet under design conditions and different quantities: Coriolis acceleration and rotary stagnation pressure, will be displayed to investigate the sources of the flow deviation. Four geometries will be drawn with different number of blades with the aim to propose a least-square fitting curve, which correlates the turbine slip factor and the number of blades.

Finally, the presence of a vaneless distributor is taken into account showing its impact on the flow deviation at the inlet of the runner and on the specific work calculation. As presented in previous works [14, 15], this kind of correlation is helpful to predict the performance of PaTs [16], but also in designing novel radial runner for specific applications.

GEOMETRY AND NUMERICAL DOMAIN

The geometry studied in this work is a simplified reconstruction of the purely radial impeller of an electrical submersible pump investigated by Monte Verde et al. [17]. The electrical submersible pump, typically called an ESP, is an efficient and reliable artificial-lift method for lifting moderate to high volumes of fluids from wellbores.

As explained by Brennen [18] in a centrifugal machine with purely radial flow, a cross-section of the flow would be as shown in Figure 1(a), an array known as a "radial cascade". In a simple radial cascade, the blade angle, $\beta_b = 90 - \beta'$, is uniform along the length of the blades, see Figure 1 and 2.

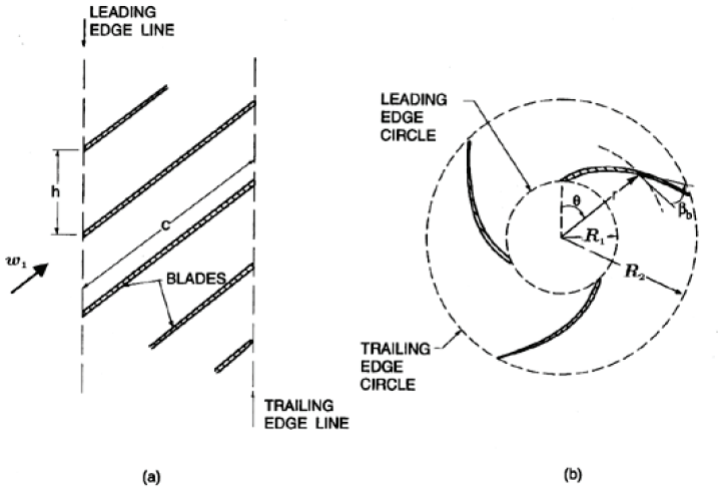

FIGURE 1. Representation of radial cascade by C.E. Brennen [18].

The resulting blade geometry is known as a logarithmic spiral, the coordinates of the blades being given by the equation:

$$\theta - \theta_0 = A \ln r \tag{1}$$

where $A = \cot(\beta')$ and θ_0 are constants. Logarithmic spiral blades are therefore equivalent to straight blades in a linear cascade.

In this work, the c_{line} of the blades has been designed according to a logarithmic spiral law. In polar coordinates (r,θ) the logarithmic curve can be written as:

$$r = ae^{b\theta} \tag{2}$$

With the purpose to follow the shape of the ESP described by Monte Verde et al. [17] the positive real constants a and b have been defined once known the dimensions of the runner. Fixed the curve initial (R_1) and final (R_2) conditions, a and b result equal to 0.0235 and 0.7585, respectively. Moreover, γ which is the difference between the initial and the final polar coordinate θ has been imposed as follows:

$$\gamma = \theta_2 - \theta_1 = 80^\circ. \tag{3}$$

The logarithmic spiral is a self similar curve being the locus of points in which the angle β' between the tangent and the radial line is constant (Figure 2) since:

$$\tan\beta' = \frac{rd\theta}{dr} = \frac{1}{b} \tag{4}$$

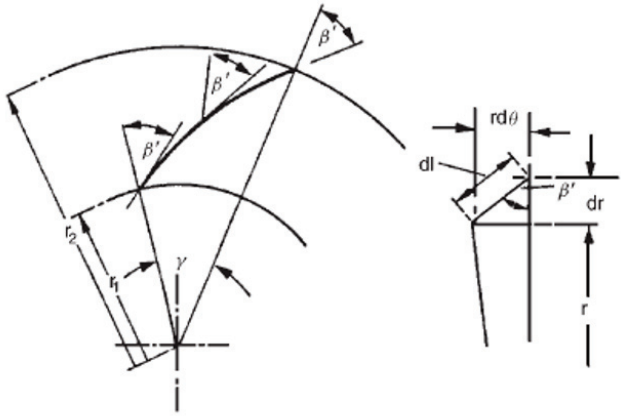

FIGURE 2. Properties of the logarithmic spiral law.

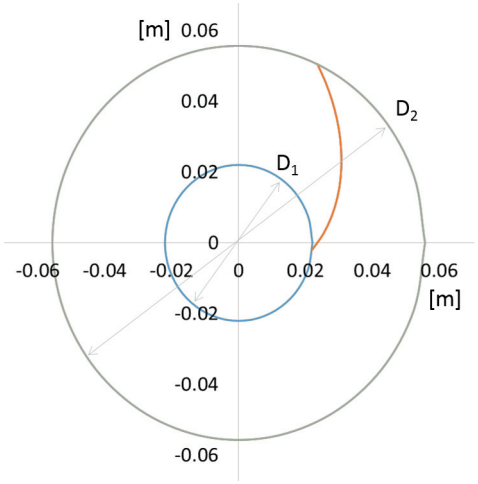

FIGURE 3. Representation of the logarithmic spiral (orange) and the inner (blue) and outer (grey) diameter of the impeller investigated by Monte Verde et al. [17].

The curve obtained by applying the equations and constants previously described is displayed in Figure 3, it starts from the outer diameter (D_2) and ends in correspondence of the inner diameter (D_1).

Using this criterion, 4 geometries characterized by different numbers of zero-thickness blades (i.e., 3, 7, 14 and 28) have been designed. Unstructured meshes have been generated by means of the Icem CFD code. The number of nodes has been chosen to guarantee a good level of refinement for the blade curvature. Moreover, the node spacing has been kept proportional for each edge in order to obtain the same grid density. The blade node number is 111, while the arcs have been discretized with an angular node spacing equal to 0.5°. In all the four cases the geometry consists of the vane, delimited by the spiral logarithmic blades, and a short outlet pipe, see Figure 4. The inlet and the outlet surfaces are cylindrical surface and the radius of the domain outlet (red arc in Figure 4) has been set as $0.27R_2$. The

main dimensions and geometry information are summed up in Figure 4 and Table 1, where φ is the flow coefficient defined as w_{r2}/u_2.

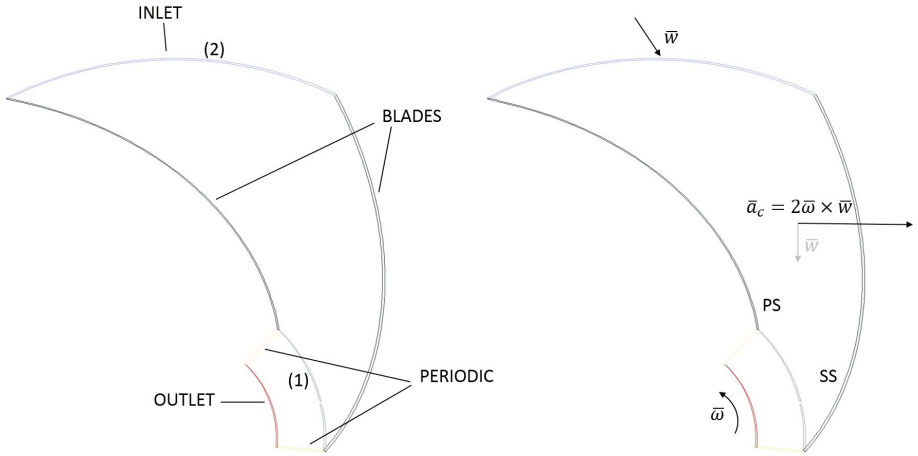

FIGURE 4. On the left, numerical domain and boundary conditions. On the right, representation of the pressure (PS) and suction (SS) sides with an example of the Coriolis acceleration vector ($\overline{a}_c$).

TABLE 1. Main dimensions of the runner.

R_2 [mm]	R_1 [mm]	β_2 [°]	β_1 [°]	n [rpm]	φ [-]
55.70	22.05	37.2	37.2	3500	0.098

GOVERNING EQUATIONS

The simulations have been performed with the commercial software Ansys FLUENT. Steady-state results have been obtained by solving the equations in a relative reference frame under inviscid flow conditions. The inviscid flow analysis neglects the effect of viscosity on the flow and is appropriate for high-Reynolds-number applications where inertial forces dominate over viscous forces. The mass conservation equation (5) is the same as for a laminar flow, but the momentum conservation equations (6) is reduced due to the absence of molecular diffusion.

Simulations have been performed with a second-order accurate scheme for the continuity, Equation 5, and the momentum equations, Equation 6.

$$\nabla \cdot \overline{v} = 0 \tag{5}$$

$$\nabla \cdot (\rho \overline{v}\overline{v}) = -\nabla p \tag{6}$$

where v is the absolute velocity vector and p the static pressure. Rearranging the Equation 6 in the rotating reference frame in terms of the relative velocity vector (w) leads to:

$$\nabla \cdot (\overline{w}\overline{w}) + 2\overline{\omega} \times \overline{w} = -\nabla\left(\frac{p}{\rho}\right) + \nabla\left(\frac{\omega^2 r^2}{2}\right) \tag{7}$$

where w is the relative velocity and ω is the angular velocity of the relative reference frame. Regarding the boundary conditions, uniform velocity components have been imposed at the inlet of the domain (2) and uniform pressure distribution at the outlet (red arc), see Figure 4. A shot pipe has been added downstream the vane outlet (1) in order avoid the influence of the constant pressure boundary condition on the development of flow deviation.

RESULTS AND DISCUSSION

Firstly, the performance of the radial impeller has been calculated by means of the infinite-blade theory. The specific work, Y, calculated by Equation 8 according to Euler's equation, is equal to 351.46 J/kg at a flow rate $Q = 15.2\ m^3/h$ and rotational speed $n = 3500\ rpm$. The specific speed ($n_q = n\sqrt{Q}/H^{0.75}$) results equal to 15.5.

$$Y = u_2 c_{u2} - u_1 c_{u1} \tag{8}$$

When calculating the turbomachinery performance, by applying the theorem of conservation of momentum, only the average velocities prevailing at the chosen control surfaces are considered. Thus, the value of c_{u1} and c_{u2} obtained via CFD simulations have been calculated as mass-weighted averages. Under the hypothesis of inviscid flow, the flow deviation is caused by the inertial effects which are represented in Figure 4. Moreover, for irrotational flows (Equation 9) a flow deviation is expected downstream of the vane outlet since a counter rotating vortex, which is superimposed to the main flow, develops inside the vane. Ventrone [19] was one of the first to focus on slip phenomenon in centripetal turbomachines in the early 70s, claiming that Busemann's results [4], obtained for centrifugal flows into radial blade vanes, are also valid for centripetal flows. As shown by Ventrone [19] and Shi et al. [20], under the hypothesis of an irrotational flow without viscous effects, the Vavra's expression leads to Equation 9 [21], which points out that the flow inside a blade channel in a rotating machine is subject to a counter rotating vortex with an intensity equal to:

$$\nabla \times \overline{w} = -2\overline{\omega} \tag{9}$$

In order to investigate the inertial forces the contours of the Coriolis acceleration ($\overline{a}_c = 2\overline{\omega} \times \overline{w}$) have been plotted and compared (Figure 5). The results show that for low number of blades higher localized effect of the inertial phenomena are observed. The results show a different field of a_c due to the fact that the pressure field around the blades and therefore the velocity are more homogeneous when the number of blades is high. This is pointed out by curves with constant radial coordinate plotted in Figure 5. For high number of blades, a_c rises from the inlet towards the outlet keeping its value constant along constant radial coordinate inside the vane; conversely, for low number of blades a_c shows a region gradually extended where a_c reaches its maximum, in particular close to the pressure side (PS) of the blade.

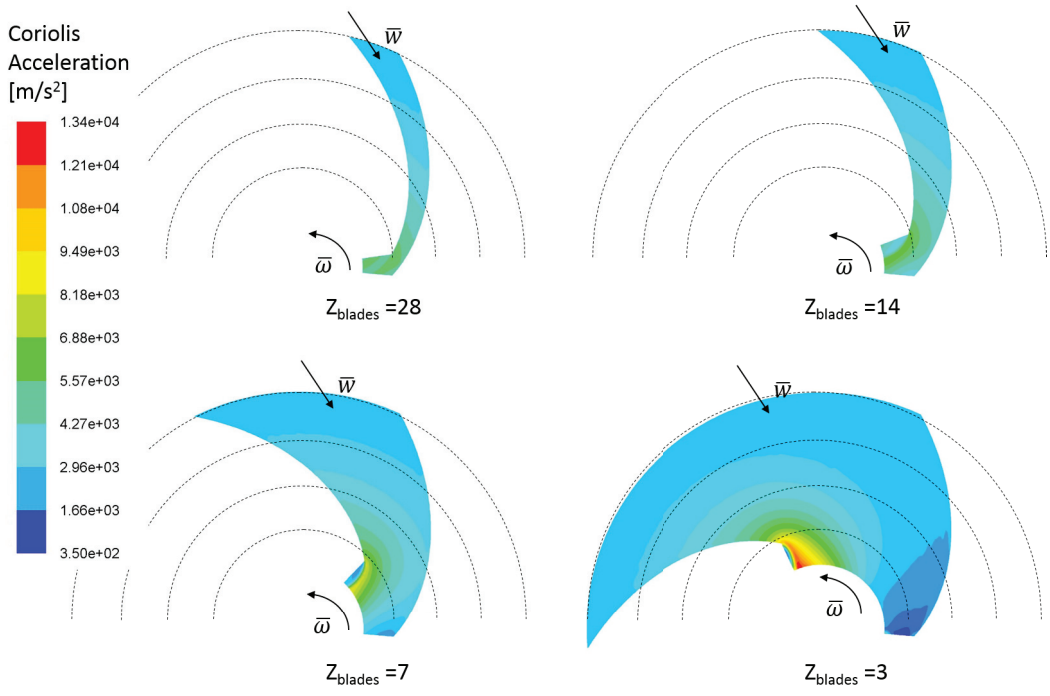

FIGURE 5. Comparison of Coriolis acceleration contours by varying the number of the blades.

A pressure gradient develops inside the vane to balance the Coriolis acceleration as evidenced by Equation 10:

$$2\omega w_r = -\frac{1}{\rho}\frac{\partial p}{r\partial\theta} \tag{10}$$

which is the projection of Equation 7 onto θ direction. If we consider that the left hand side of Equation 10 is constant (ω is constant and the geometry and the blade angles are the same), the pressure gradient will be constant, but a great pressure variation will occur when the distance between two blades is larger. This means that a larger pressure gradient will deflect more significantly the velocity vector in open field region. By considering the Equation 10, the centrifugal forces do not have any effect on the tangential direction where they are null.

Another quantity which can be useful to investigate the flow deviation is the rotary stagnation pressure, p^*, Equation 11 [22]. For incompressible, inviscid flow in a rotational reference frame, the value of p^* is constant along a streamline. For the viscous flow, the change of this parameter between two points on the same streamline is due to the viscous losses. The dimensionless rotary stagnation pressure (p^*_{adim}, Equation 12) has been calculated and plotted, see Figure 6. It can be seen that the streamlines keep their value constant from the inlet to the outlet, since the solver is inviscid. Nevertheless, the streamlines, colored by p^*_{adim}, show a curvature in the same direction of the peripheral velocity immediately downstream of the vane outlet: low blade number implies high curvature intensity. Moreover, the streamlines deviation (Figure 6) occurs in the same region where the inertial effects reach their maximum (Figure 5). In the open region, it is clear that the value of the rotary stagnation pressure undergoes a change where two streamlines, coming from the pressure and the suction sides, get in contact at the blade trailing edge .

$$\frac{p^*}{\rho} = \frac{p_{st}}{\rho} + \frac{w^2}{2} - \frac{u^2}{2} \tag{11}$$

$$p^*_{adim} = \frac{p^* - p^*_{min}}{p^*_{max} - p^*_{min}} \tag{12}$$

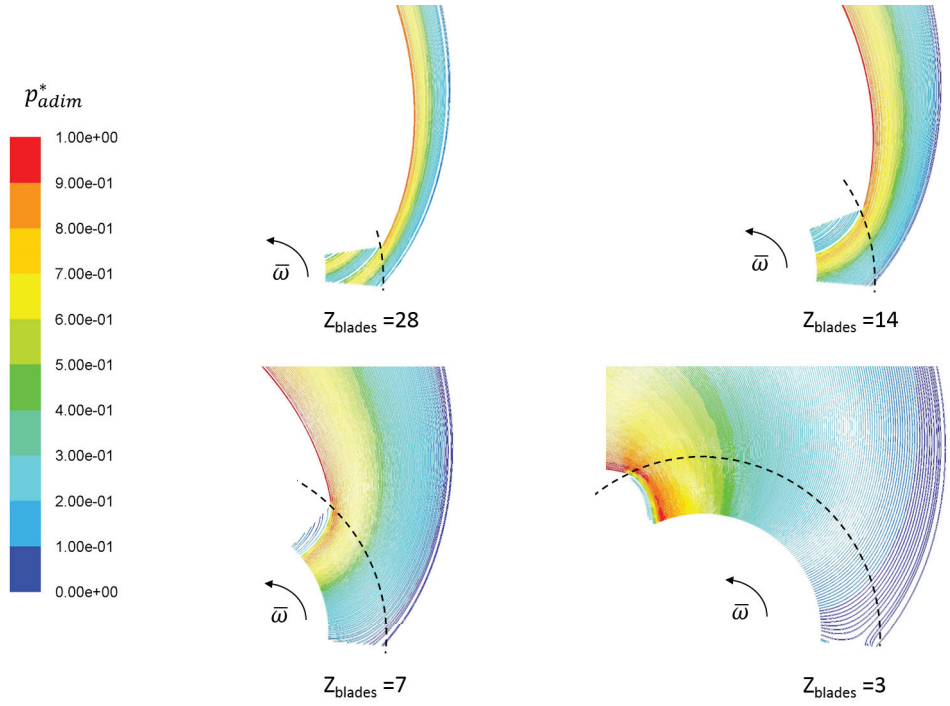

FIGURE 6. Streamlines colored by dimensionless rotary stagnation pressure, p^*_{adim}, Equation 12.

In Figure 7 $c_{u1,th}/c_{u1}$ at the outlet (1) of the 4 geometries for two rotational speeds (n = 3500 and 900 rpm) has been calculated and plotted. The two curves for the two rotational speed are overlapped. This is clear if we consider

that the impeller geometry is the same and the operating conditions are in fluid dynamic similitude, namely the two geometries are in geometrical and kinematic similarity (similarity laws). The absolute tangential velocity undergoes different levels of deviation by varying the number of blades. Indeed, its deviation goes from 298% to 39%. In table 2, it can be seen that even though the level of absolute velocity deviation is high, the head (H) calculated by means of the Euler's formula (Equation 13) returns lower deviations than one expects (-10%). Indeed, the absolute velocity components at the inlet (2) are larger than those at the outlet (1).

$$H = \frac{u_2 c_{u2} - u_1 c_{u1}}{g} \tag{13}$$

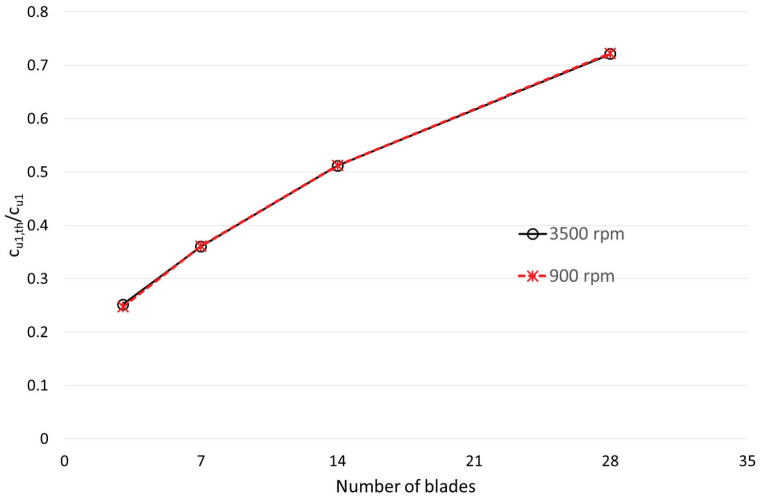

FIGURE 7. Evolution of the theoretical value over the absolute tangential velocity calculated via CFD ($c_{u1,th}/c_{u1}$) for two different rotational speed.

With the purpose to evaluate such deviation, the turbine slip factor has been defined as follows:

$$\sigma = \frac{Y_{CFD}}{Y_{th}} \tag{14}$$

where Y is the specific work defined in Equation 8, and the subscripts CFD and th refers to values obtained via computational fluid dynamics and theoretical calculi, respectively.

TABLE 2. Value of the head (H), absolute tangential velocity (c_{u1}) and turbine slip (σ) for a purely radial impeller with low specific speed (n_q).

	3 blades	**7 blades**	**14 blades**	**28 blades**	**theoretical**
H [m]	32.42	33.80	34.74	35.39	35.83
σ	0.905	0.943	0.969	0.987	-
c_{u1} [m/s]	5.53	3.86	2.72	1.93	1.39
c_{u1} [% err]	298	178	96	39	-

The influence of the slip, and therefore the inertial effects, is not negligible inside radial runners, see Table 2. Eventually, based on the computed values, least-square fitting curve (Equation 15), which allows the calculation of the slip for radial runners with low specific speed, is proposed (coefficient of determination R^2=0.9864):

$$\sigma = 0.0373 \ln(Z_{blades}) + 0.8671 \tag{15}$$

Influence of a vaneless distributor

At the end of this investigation, the importance of taking into account the slip phenomenon in predicting the performance of radial pumps operating as turbines has been assessed. In order to evaluate the influence of the slip phenomenon at the inlet of the runner under design conditions, a geometry with a vaneless distributor (3) has been studied, see Figure 8. For this application the 7 bladed runner has been modified. The outer distributor radius (R_3) is equal to 0.07 m and its walls are parallel.

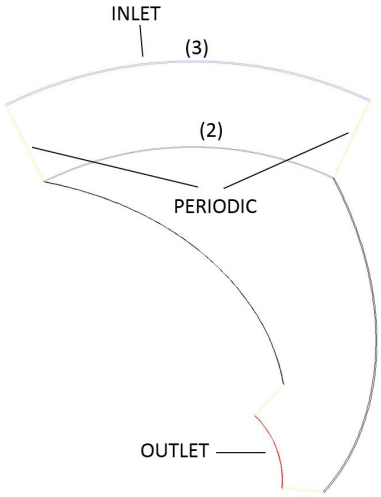

FIGURE 8. Representation of numerical domain with the vaneless distributor.

A uniform velocity boundary condition has been imposed at its inlet and periodic boundary conditions have been imposed along the radial surfaces which connect the runner inlet (R_2) with the distributor inlet (R_3).

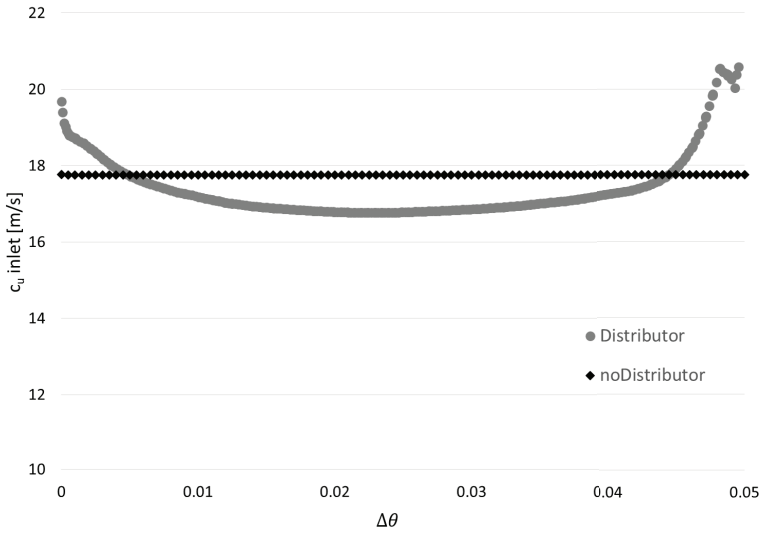

FIGURE 9. Representation of absolute tangential velocity (c_u) at the inlet of the domain for the 2 geometries (with and without distributor).

The results point out that the mean value of the tangential velocity (c_u) at the vane inlet section (2) is the same in the two case (with and without distributor), see Figure 9. In Figure 9 and 10, $\Delta\theta = 2\pi R_2/Z_{blades}$, namely it is a

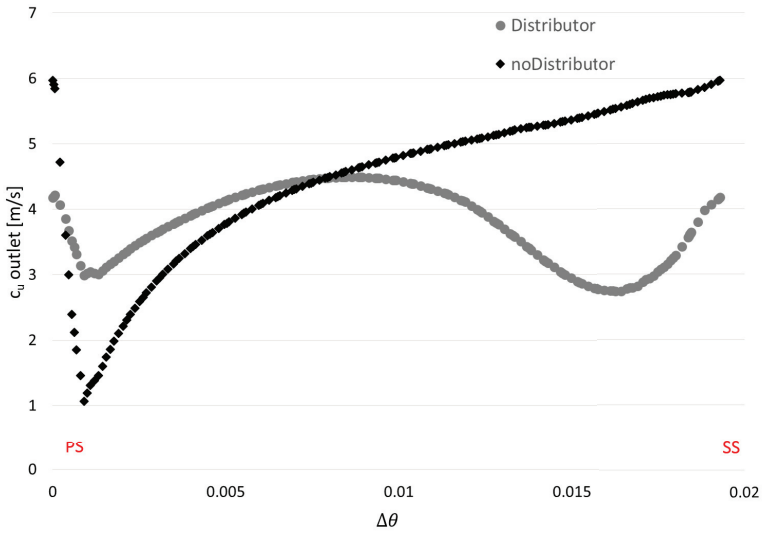

FIGURE 10. Representation of absolute tangential velocity (c_u) at the outlet of the vane for the 2 geometries (with and without distributor).

fraction of the arc length. Moreover, their mean value is equal to the theoretical one ($c_{u2,th} = 17.76\ m/s$). On the other hand, the tangential velocities at the vane outlet display slightly different trends in the two cases. Again their mean values are comparable but quite different from the theoretical one, see Table 2. It can also be seen that their tangential distribution is different in some parts. In Figure 10 it can be seen that the flow deviation is mainly localized between the pressure and the suction side for the zero thickness blade. This means that, about the geometry considered here and similar specific speed impellers, the slip phenomenon at the vane inlet does not affect the Euler's work calculation, conversely in both the cases the absolute tangential velocity at the outlet shows a global deviation which reduces the work exchanged by the fluid. In the future work, the application of the same methodology will be carried out to evaluate the slip phenomenon inside mixed-flow impeller vanes where more complex phenomena are involved.

CONCLUSIONS

In this work a simplified ESP (Electrical Submersible Pump) has been considered in order to investigate by means of numerical simulations the effect of the inertial forces on the slip phenomenon at its outlet under turbine operating mode. The runner geometry consists of zero-thickness spiral logarithmic blades. The geometry is purely radial, thus the flow direction is composed of tangential and radial components, simplifying the discussion about the forces involved and the results. Four different geometries have been considered with different numbers of blades (Z_{blades}= 3, 7, 14 and 28) and the domains have been discretized with unstructured grids. The number of blades has been varied on purpose in order to correlate the flow deviation with the number of blades. The results show a strong dependency of the absolute tangential velocity with respect to the number of blades, as expected. Furthermore, a non-negligible deviation affects the work extracted by the runner, thus a least-fitting curve which correlates the turbine slip with the number of blades has been proposed. A quantitative analysis has been performed by comparing the contours of the Coriolis acceleration and the streamlines colored by the dimensionless rotary stagnation pressure. Finally, the influence of the slip phenomenon at the inlet of the runner has been investigated by adding a vaneless distributor upstream the runner. The result is that the slip phenomenon negligibly affects the value of the incoming absolute tangential velocity vector. In the future work, the application of the same methodology will be carried out to evaluate the slip phenomenon inside mixed-flow impeller vanes with the aim to propose a more general correlation which includes different number of blades and specific speeds.

REFERENCES

[1] A. Stodola, *Steam and Gas Turbines* (McGraw-Hill, New York, 1945).

[2] P. C., *Die Kreiselpumpen fr Flssigkeit en und Gase* (1983).

[3] W. F.J., Trans. ASME: J. Eng. Gas Turbines Power **89**, 558–566 (1967).

[4] A. Busemann, J. Appl. Math. Mech. **8**, p. 372384 (1928).

[5] J. Gülich, *Centrifugal Pumps* (Springer Berlin Heidelberg, 1, 2014).

[6] S. L. Dixon, *Fluid Mechanics: Thermodynamics of Turbomachinery* (Elsevier, 1966).

[7] M. Stefanizzi, F. Torresi, Marco Fornarelli, B. Fortunato, and S. M. Camporeale, "Performance prediction model of multistage centrifugal pumps used as turbines with two-phase flow," in *Energy Procedia*, ATI 2018 - 73nd Conference of the Italian Thermal Machines Engineering Association (Elsevier, 2018), pp. 408–415.

[8] M. Renzi, P. Rudolf, D. Štefan, A. Nigro, and M. Rossi, Applied Energy **250**, 665–676 (2019).

[9] M. Binama, W.-T. Su, X.-B. Li, F.-C. Li, X.-Z. Wei, and S. An, Renewable and Sustainable Energy Reviews **79**, 148–179 (2017).

[10] M. Stefanizzi, T. Capurso, G. Balacco, M. Torresi, B. Mario, P. Ferruccio, B. Fortunato, and S. M. Camporeale, "Preliminary assessment of a pump used as turbine in a water distribution network for the recovery of throttling energy," in *Proceedings of 13th European Turbomachinery Conference on Turbomachinery Fluid Dynamics and Thermodynamics, ETC* (2019).

[11] T. Capurso, L. Bergamini, S. M. Camporeale, B. Fortunato, and M. Torresi, "Cfd analysis of the performance of a novel impeller for a double suction centrifugal pump working as a turbine," in *Proceedings of 13th European Turbomachinery Conference on Turbomachinery Fluid Dynamics and Thermodynamics, ETC* (2019).

[12] T. Capurso, M. Stefanizzi, S. Ranaldo, S. M. Camporeale, B. Fortunato, and M. Torresi, Water **11** (2019).

[13] W. Xiaohui, Y. Junhu, and X. Zhengting, Fluids Engineering Division Summer Meeting **1A**, p. 1 (2017).

[14] T. Capurso, M. Stefanizzi, M. Torresi, G. Pascazio, G. Caramia, S. M. Camporeale, B. Fortunato, and L. Bergamini, "How to improve the performance prediction of a pump as turbine by considering the slip phenomenon," in *EWaS 3*, Proceedings 2(11) (MDPI, 2018).

[15] M. Stefanizzi, T. Capurso, M. Torresi, G. Pascazio, S. Ranaldo, S. M. Camporeale, B. Fortunato, and R. Monteriso, "Development of a 1-d performance prediction model for pumps as turbines," in *EWaS 3*, Proceedings 2(11) (MDPI, 2018).

[16] M. Stefanizzi, M. Torresi, B. Fortunato, and S. M. Camporeale, "Experimental investigation and performance prediction modeling of a single stage centrifugal pump operating as turbine," in *Energy Procedia*, ATI 2017 - 72nd Conference of the Italian Thermal Machines Engineering Association (Elsevier, 2017), pp. 589 – 596.

[17] W. M. Verde, J. L. Biazussi, N. A. Sassim, and A. C. Bannwart, Experimental Thermal and Fluid Science **85**, 37–51 (2017).

[18] C. E. Brennen, *Hydrodynamics of Pumps* (Cambridge University Press, Cambridge, 2011).

[19] G. Ventrone, L'Energia Elettrica **9** (1972).

[20] G. Shi, X. Liu, J. Yang, and J. Miao, S.and Li, Adv. Mech. Eng. **7** (2015).

[21] M. H. Vavra, *Aerothermodynamics and Flow in Turbomachines* (John Wiley & Sons, New York, 1960).

[22] M. J. Johnson MW, "The influence of flow rate on the wake in a centrifugal impeller," in *ASME. J. Eng. Power.*, 105 1 (ASME, 1983), pp. 33–39.